Journal of Power Sources 457 (2020) 228042

Contents lists available at ScienceDirect

Journal of Power Sources

journal homepage: www.elsevier.com/locate/jpowsour

Effect of carbon surface on degradation of supercapacitors in a negative potential range

Rui Tang [a], Masanori Yamamoto [a], Keita Nomura [a], Emilia Morallón [b], Diego Cazorla-Amorós [b], Hirotomo Nishihara [a,*], Takashi Kyotani [a]

[a] Institute of Multidisciplinary Research for Advanced Materials, Tohoku University, 2-1-1 Katahira, Aoba-ku, Sendai, Miyagi, 980-8577, Japan
[b] Departamento de Química Inorgánica e Instituto Universitario de Materiales, Universidad de Alicante, Apartado 99, 03080, Alicante, Spain

HIGHLIGHTS

- The corrosion mechanism at a negative electrode of supercapacitors is investigated.
- Corrosion reactions are found to occur at the carbon basal plane rather than edge sites.
- The theoretical calculation also supports the higher reactivity of the carbon basal plane.

GRAPHICAL ABSTRACT

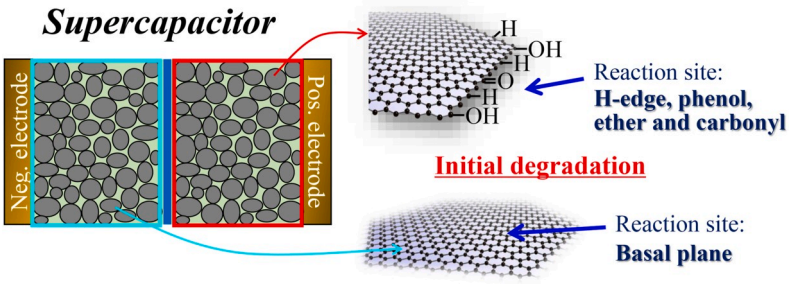

ARTICLE INFO

Keywords:
Supercapacitors
Electrochemical degradation
Negative potential range
Edge site
Basal plane

ABSTRACT

The stability of supercapacitors is the key factor for their use under high temperature, high voltage and long-term durability. To improve the supercapacitor stability, there is a need to understand the degradation mechanism. In this work, the degradation sites in a carbon electrode at negative potential range are investigated in two common organic electrolytes: 1 M Et_4NBF_4 dissolved in propylene carbonate and in acetonitrile. To elucidate the common factor over a wide range of carbon materials, we examined eight kinds of carbon materials including activated carbons, carbon blacks, zeolite-template carbon (high surface area and a large amount of carbon edge sites) and graphene mesosponge (high surface area and a little amount of carbon edge sites). Their surface structures are distinguished into two regions: carbon basal planes and edge sites by nitrogen physisorption and high-sensitivity temperature-programmed desorption up to 1800 °C. Unlike the degradation at positive potential range, initial degradation reactions at negative potential range occur mainly on the carbon basal planes rather than the edge sites. This finding is corroborated by the theoretical calculation.

1. Introduction

Electric double-layer capacitors, also known as supercapacitors, are energy storage devices based on reversible electrostatic adsorption of ions on the electrolyte-electrode interface [1]. Supercapacitors have features of high power density and long cycle life [2], and have been widely used in automobiles, backup systems [3], screwdrivers, and electric cutters [4]. For most commercial supercapacitors, activated

* Corresponding author.
E-mail address: hirotomo.nishihara.b1@tohoku.ac.jp (H. Nishihara).

https://doi.org/10.1016/j.jpowsour.2020.228042
Received 5 October 2019; Received in revised form 12 February 2020; Accepted 12 March 2020
Available online 19 March 2020

carbons with high surface area (~2000 $m^2 g^{-1}$) are used as electrode in combination with organic electrolytes. Organic electrolytes such as tetraethylammonium tetrafluoroborate (Et_4NBF_4) dissolved in propylene carbonate (PC) or in acetonitrile (AN) are commonly selected for their low viscosity and relatively wide potential window which are beneficial for better rate capability and large energy density, respectively. Supercapacitors using these organic electrolytes usually operate within a certain voltage range (<2.8 V) and temperature range (−40 to 70 °C) to avoid degradation reactions that cause capacitance drop [5], resistance increase [5], and gas evolution [6]. Nevertheless, the degradation reactions progress very slowly such that supercapacitors have a finite life of 500,000 to 1,000,000 cycles [2], depending on operating temperature [7–9]. It is generally known that an increase of 10 °C halves the life of supercapacitors around room temperature. Thus, the improvement of the supercapacitor stability is an important issue in the industry for extending both the cycle life and operating temperature range [10]. Moreover, better stability enables the expansion of voltage range which is important from two standpoints. First, the increase of working voltage (V) achieves higher energy density (E), according to $E = CV^2/2$, where C is capacitance. Second, by increasing V of a single cell, fewer cell-stacking units are needed in high-voltage modules enabling the development of compact devices [8,11].

To improve supercapacitor stability, it is crucial to understand the degradation reaction mechanism. It is known that severe degradation reactions produce gases [6,12,13] and deposit polymers at the interface of carbon electrode and electrolyte [14]. The gas production increase the inner pressure of supercapacitor risking cell breakage [15]. Moreover, the polymer deposition increases the inner cell resistance and block carbon nanopores, declining capacitance [5,16]. On the electrolyte side, many groups have observed the decomposition of electrolyte solvents [2,6,17,18] and electrolyte salts [5,17,19,20] based on the results obtained by X-ray photoelectron spectroscopy [5,17,21], nuclear magnetic resonance spectroscopy [5], infrared spectroscopy [17], gas chromatography [12,19], mass spectrometry [6], energy dispersion X-ray fluorescence spectroscopy [14], and scanning electron microscopy [14]. While most reported decomposition, very few have studied the origin of degradation reactions at the carbon electrode side in organic electrolytes. Azaïs et al. have proposed that carbon porosity does not affect the stability of supercapacitors but surface functionalities play an important role instead [5], and further supported by other groups [12,13,16]. However, the studies were performed on a limited types of carbon materials and their conclusions cannot be generalized for other carbon materials. Moreover, specific carbon sites responsible for the degradation have not been explored at the positive and negative potential ranges. Our group previously systematically investigated the effect of carbon structure (porosity, crystallinity, radicals and edges) on the initial degradation reactions at the positive potential range. We have elucidated that the degradation-causing sites in carbon materials are carbon edge sites terminated by hydrogen (H) or oxygen (O) in the forms of phenol, ether, and carbonyl groups [18].

To complement the previous study on the initial degradation reactions at the positive potential range, this work focuses on the initial degradation reactions at the negative potential range in two commonly used electrolyte solutions, Et_4NBF_4/PC and Et_4NBF_4/AN. To elucidate the degradation-causing sites common to a variety of different carbon materials, we selected eight different carbon materials including four activated carbons, two carbon blacks, zeolite-template carbon (ZTC; high surface area and a large amount of carbon edge sites) [22] and graphene mesosponge (GMS; high surface area and a small amount of carbon edge sites) [23]. Since the degradation reactions occur at the interface of carbon and the electrolyte solution, the degradation-causing sites must exist on the carbon surface. However, we have previously found that the specific surface area has almost no correlation with the degradation at the positive potential range [18]. In this work, we revisited the effect of specific surface area and found that the surface area corresponding to the carbon basal planes (but not to the edge planes) indeed affects the degradation reactions at the negative potential range. The different reactivities on the basal planes and the edge sites are further explored with theoretical calculations.

2. Methods

2.1. Carbon materials

Eight kinds of carbon materials were used in this work including four kinds of activated carbons, two kinds of carbon blacks, ZTC [22] and GMS [23]. Details of the carbon materials are listed in Table 1. Activated carbons (Fig. 1a) are highly porous as they are mainly composed of disordered sp^2-hybridized carbon frameworks guided by the carbon precursors and preparation conditions. Carbon blacks (Fig. 1b) are spherical particles of stacked small carbon layers with diameters of several tens nanometers [24]. Carbon blacks have a smaller amount of carbon edge sites and smaller surface area than activated carbons. ZTC (Fig. 1c) is an ordered microporous carbon comprised of single-layer graphene framework with the highest surface area in Table 1 and a very large amount of edge sites. GMS (Fig. 1d) is made up of curved single-walled graphene with a very small amount of carbon edge sites.

2.2. Characterization

Nitrogen adsorption isotherms of the carbon materials were measured at −196 °C by using a BELSORP-max instrument (MicrotracBEL Corp.). The specific surface area (S_α) was calculated by the subtracting pore-effect method [25] based on the α_s-plot. Since S_α provides accurate surface area without the effect of micropore filling, it is more reliable especially for microporous materials than the one calculated by the Brunauer–Emmett–Teller method (called BET surface area) [26]. The carbon edge sites were characterized by the high-sensitivity TPD method which had been developed by our group [27]. During the TPD measurement, ca. 1 mg of carbon material was heated up to 1800 °C

Table 1
A list of the eight carbon materials used in this work.

Sample	Supplier	S_α [a] [$m^2 g^{-1}$]	N_{edge} [b] [mmol g^{-1}]	Remarks
YP50F	Kuraray Chemical Co., Ltd.	1731	5.6	A coconut-shell-derived steam-activated carbon which is used for commercial supercapacitors
AAC	home made [37]	2512	4.1	An anthracite-derived KOH-activated carbon
AACH2	home made [16]	2363	3.3	AAC treated with H_2 at 850 °C for 1 h
MSC30	Kansai Coke and Chemicals Co., Ltd.	2662	2.3	A KOH-activated carbon, also known as MAXSORB®
XC72	Cabot Co., Ltd	243	1.0	Porous carbon black (VULCAN XC72)
KB	Lion Specialty Chemicals., Ltd	776	2.2	Hollow carbon black (Ketjen Black EC-300 J)
ZTC	home made [22]	3345	15.4	Zeolite-templated carbon with high surface area and a large amount of edge sites
GMS	home made [23]	1708	0.1	Graphene mesosponge with high surface area and a very small amount of edge sites

[a] Specific surface area calculated by the subtracting pore-effect method [25] based on the α_s-plot.
[b] Amount of edge sites (N_{edge}) calculated by using the TPD results. Details can be found in 2.2. Characterization.

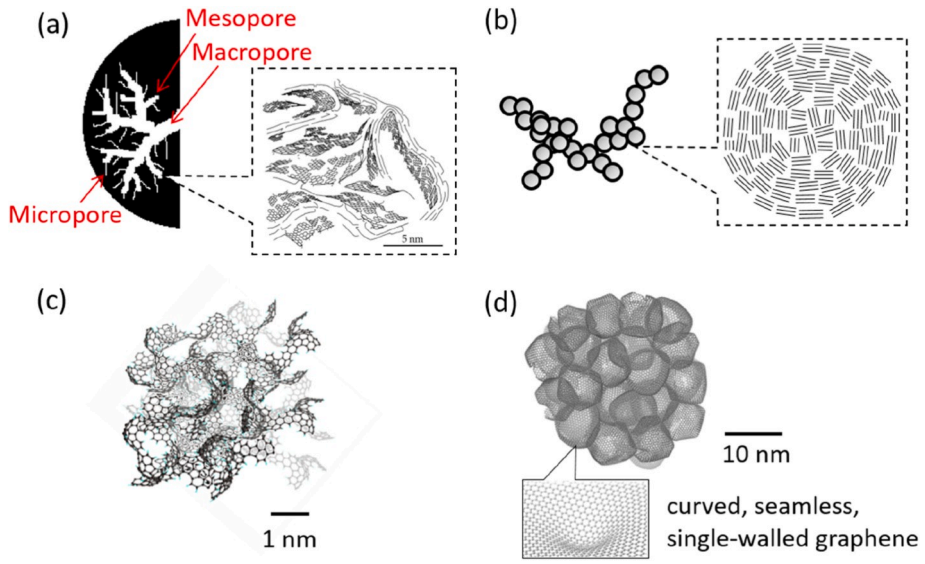

Fig. 1. Structure models of carbon materials used in this work. (a) Activated carbon, (b) carbon black, (c) zeolite-template carbon and (d) graphene mesosponge.

at a rate of 10 °C min^{-1} under high vacuum (ca. 1×10^{-5} Pa). The H-terminated sites and oxygen functional groups at carbon edge sites were thermally decomposed into H_2, H_2O, CO_2 and CO gases and quantified by a mass spectrometer [18]. Since almost all the edge sites terminated by H or oxygen functional groups are decomposed as the aforementioned gases below 1800 °C, it is possible to calculate the total amount of these edge sites (N_{edge} [mmol g^{-1}]) according to the following equation:

$$N_{edge} = N_{CO} + N_{CO2} + N_{H2O}(>400\ °C) + 2 \times N_{H2} \quad (1)$$

where N_{CO}, N_{CO2}, and N_{H2} are desorption amounts (mmol g^{-1}) of CO, CO_2, and H_2, respectively, during the TPD measurement. N_{H2O}(>400 °C) is the H_2O desorption amount in TPD above 400 °C. H_2O desorption below 400 °C corresponds to physisorbed water or the desorption by dehydration of two carboxyl groups [18]. A coefficient of 2 is assigned to N_{H2} as 1 mol of H_2 originates from 2 mol of H-terminated edge sites. Since H_2 may also originate from phenol groups (H-terminated edge sites are left after the thermal decomposition of phenols as CO gases), the calculation of N_{edge} may be an overestimate as the phenol groups are doubly counted. According to our calculation (shown in Fig. S1 and Table S1), this overestimation has a miniscule effect on the calculation of N_{edge}, and we thus neglect the effect. On the same note, free edge sites like σ-radicals and triplet carbenes [28] are not considered in equation (1), thus N_{edge} may be underestimated. In order to estimate the amount of free edge sites, we compared N_{edge} with our previous results obtained by magnetic susceptibility measurement which can determine the spin density in the used carbon materials [18]. There are three possible origins for spin, including σ-radicals, triplet carbenes and π-radicals [29]. Considering the high reactivity of σ-radicals and the fact that the carbons we used are exposed in air, it is reasonable to ascribe most of the observed spin to triplet carbenes and π-radicals. However, the presence of π-radicals does not cause the underestimation of N_{edge}, because π-radicals are always formed at H-terminated edge sites and can be detected by TPD. The maximum amount of free edge sites can be calculated by assuming all the spin comes from triplet carbenes. However, according to our calculation (shown in Table S2), this underestimation is very small for the calculation of N_{edge}. By using the resulting N_{edge}, we then estimated the edge-site surface area (S_{edge}) by assuming that the area occupied by each edge site is 0.083 nm^2 [30]. By subtracting S_{edge} from S_{α}, basal-plane surface area (S_{basal}) was calculated and they are shown in Table 2.

Table 2
Surface areas of carbon materials used in this work.

Sample	S_{edge} [m^2 g^{-1}][a]	S_{basal} [m^2 g^{-1}][b]
YP50F	277	1454
AAC	205	2307
AACH2	165	2198
MSC30	115	2547
XC72	52	191
KB	107	669
ZTC	768	2577
GMS	7	1701

[a] Edge-plane area calculated by using the results of N_{edge} and assuming that the area occupied by each edge site is 0.083 nm^2.
[b] Basal-plane surface area by subtracting S_{edge} from S_{α}.

2.3. Electrochemical measurement

The irreversible process occurring on carbon electrode was quantitatively characterized by cyclic voltammetry (CV) with a three-electrode cell at 25 °C [31]. A working electrode was prepared in the following manner: a carbon sample was mixed with a binder polymer (PTFE; PTFE 6-J, Du Pont-Mitsui Fluorochemicals Co. Ltd.) and a conductive additive (Denka black, Denki Kagaku Kogyo Kabushiki Kaisha) at the weight ratio of 90:5:5. For the two carbon black samples (XC72 and KB), the sample was mixed with PTFE at the weight ratio of 85:15 without the conductive additive, since carbon blacks have enough high electric conductivity. The resulting mixture was pressed into a sheet cut into a square shape (1 × 1 cm^2, 5–10 mg), and sandwiched by a Pt mesh to become a working electrode. The electrolyte was 1 M Et_4NBF_4 dissolved in PC or AN. An activated carbon fiber (Kuraray Chemical Co., Ltd., FT300-15) was used for the counter electrode, which was prepared in the same manner as the working electrode except for its loading amount (ca. 20 mg). The reference electrode was $Ag/AgClO_4$. With the three-electrode cell, CV was performed. First, CV scan (1 mV s^{-1}) was repeated four times in the potential range of −1.0 to 0 V, and then the lower potential limit was stepwisely expanded by 0.1 V down to −2.1 V. In each potential range, CV scan was repeated four times. The degradation of the carbon electrode was judged by irreversible charge (Q_{ir-neg} [C g^{-1}]) [18], calculated by the following equation:

$$Q_{ir\text{-}neg} = Q_{-} - Q_{+} \quad (2)$$

where Q_{-} and Q_{+} are the total charges during the negative-direction

scan and the positive-direction scan, respectively, in the first CV measurement at a certain potential range (an example is shown in Fig. 2a). The degradation at the positive potential range was also examined by similar CV measurements, in which the initial potential range of −0.5 to 0.5 V was stepwisely expanded to the positive potential by 0.1 V up to 1.3 V. The irreversible charge in positive potential range (Q_{ir-pos} [C g^{-1}]) was calculated by the following equation:

$$Q_{ir\text{-}pos} = Q_{+} - Q_{-} \quad (3)$$

To investigate a reactant included in the organic electrolytes, the reactivities of the electrolyte components (Et_4NBF_4, PC, and AN) were examined using a stable ionic liquid (1-Butyl-3-methylimidazolium tetrafluoroborate; $BMIMBF_4$, FUJIFILM Wako Pure Chemical Corporation) as a support electrolyte. In addition to pure $BMIMBF_4$, three test electrolytes were prepared: 0.26 M Et_4NBF_4/$BMIMBF_4$, 4.59 M PC/$BMIMBF_4$, and 5.18 M AN/$BMIMBF_4$. CV scans of these electrolytes were performed at 25 °C by using YP50F (Kuraray Chemical Co., Ltd.) as a working electrode in the same three-electrode cell set-up as described above.

2.4. Computational chemistry

Carbon basal planes and edge planes are quite different in their chemical nature; the former have abundant π-electrons while the latter are featured by covalent bonds with hydrogen or oxygen. As such, their interaction with electrochemical reactants may also be markedly different. To obtain the insight at the molecular level, the density functional theory (DFT) calculation for the pair of a carbon model and a reactant was also performed to estimate the energy level and the overlapping of each molecular orbitals. The calculations were carried out on an open-shelled carbon model (hexabenzocoronene) and acetonitrile (instead of PC or ions, AN is selected due to its simple structure which can avoid the geometry effect of reactants during the calculation) as a representative of reactant by using the Gaussian 16 package of program [32] with the range-separated hybrid functional of ωB97XD [33,34] together with 6–311++G* basis set for hydrogen, carbon and nitrogen atoms. The carbon model is negatively charged by introducing one electron to simulate the process at a negative potential range. For the geometry optimization of acetonitrile at the edge of the carbon model, the nitrogen atom was fixed within the co-plane of the carbon model. Time-dependent DFT (TD-DFT) calculation was also carried out at the same level of theory with the long-range corrected ωB97XD functional. Solvent effects were considered in an implicit solvent model COSMO [35] (or cubity PCM, CPCM) with acetonitrile as a solvent for all calculations. The frequency analyses were then carried out at the same level of theory to check whether there is an imaginary vibrational mode or not, and the results were used to determine the thermodynamics.

3. Results and discussion

3.1. Degradation behaviours of eight carbon materials

Fig. 2b and c shows the CV results of YP50F in the two organic electrolytes. In both cases, when the lower limit potential is −1.0 V *vs.* $Ag/AgClO_4$, the overall shape of CV curve is almost symmetrical to the x-axis, indicating that the current observed was derived from the reversible process, *i.e.*, electric double-layer capacitance. As the lower limit potential is expanded in the minus direction (to the left), the CV shape was gradually warped by the greater cathodic current at the low potential region, suggesting the occurrence of irreversible reactions. The same tendency was found in the other carbon samples (Figs. S2 and S3). The intensity of the irreversible reactions was quantitatively obtained as $Q_{ir\text{-}neg}$, calculated by the method shown in Fig. 2a [31].

Fig. 3 shows the change of $Q_{ir\text{-}neg}$ with the lower limit potential for the eight carbon materials. As a general tendency, $Q_{ir\text{-}neg}$ is gradually increased below −1.2 V for all the carbon materials, while the intensity of $Q_{ir\text{-}neg}$ highly depends on the type of carbon material. Also, the change of $Q_{ir\text{-}pos}$ with the upper limit potential is shown in Fig. S4. Previously, a part of the results shown in Fig. S4a is already reported by our group without the GMS and MSC30 data [18]. Commercial supercapacitors are

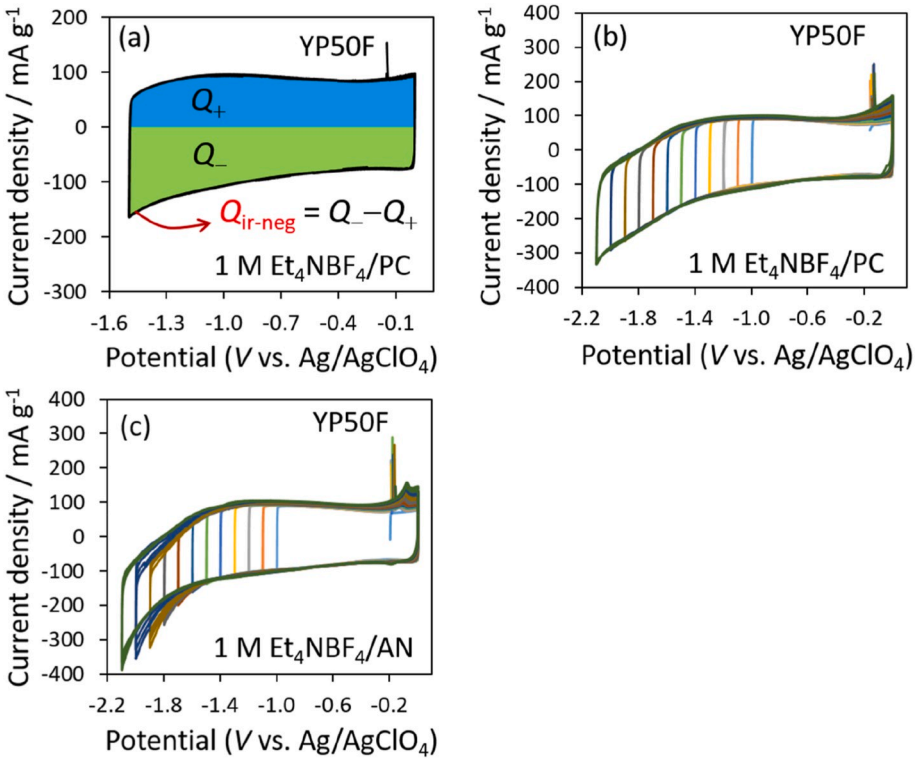

Fig. 2. (a) An example of calculating $Q_{ir\text{-}neg}$: YP50F in 1 M Et_4NBF_4/PC. (b,c) CV results of YP50F in (b) 1 M Et_4NBF_4/PC and (c) 1 M Et_4NBF_4/AN. Scan rate: 1 mV/s.

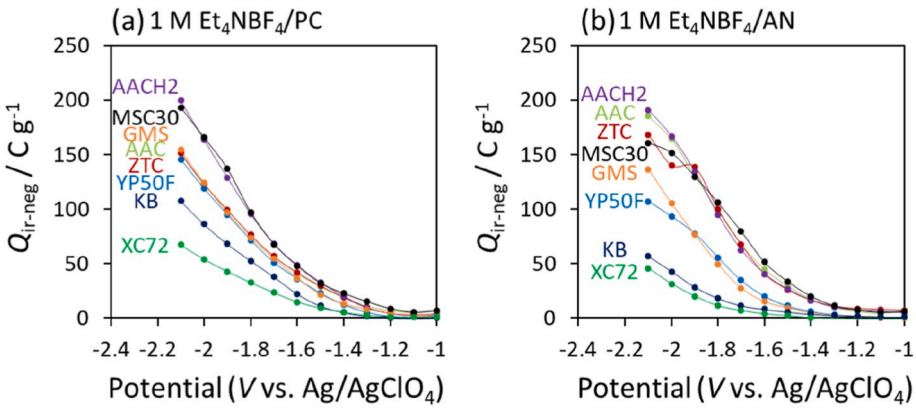

Fig. 3. The change of $Q_{ir\text{-}neg}$ depending on the lower limit potential for the eight carbon materials. Electrolytes are (a) 1 M Et_4NBF_4/PC and (b) 1 M Et_4NBF_4/AN.

usually assembled with the symmetric configuration. When the supercapacitor is charged, the potential difference of each electrode from the open circuit potential (OCP) is almost even. Considering that the OCP of the eight carbon materials is about −0.1 V vs. Ag/$AgClO_4$, the potentials of positive and negative electrodes at a fully-charged state (2.8 V for commercial supercapacitors) correspond to 1.3 and −1.5 V, respectively. Comparing Fig. 3 and Fig. S4, $Q_{ir\text{-}pos}$ at 1.3 V is much larger than $Q_{ir\text{-}neg}$ at −1.5 V for all the carbons, indicating that the degradation at the positive side was much more significant than that at the negative side. This finding is consistent with the previous reports where electrochemical degradation resulted in greater loss of porosity at the positive electrodes than that at the negative electrodes [5,16,17].

3.2. Difference in the electrochemical degradation between positive and negative potential ranges

For the degradation at the positive potential, we have previously reported a clear correlation between $Q_{ir\text{-}pos}$ and the amount of the specific edge sites which are terminated with H, phenol, ether, and carbonyl groups, expressed by $2N_{H2} + N_{CO}$ [18]. We first tried to elucidate a correlation also between $Q_{ir\text{-}neg}$ and $2N_{H2} + N_{CO}$. However, as shown in Fig. 4, correlation was not found. There is also no correlation between $Q_{ir\text{-}neg}$ and N_{CO}, N_{CO2}, N_{H2O} nor N_{H2} (Figs. S5 and S6). On the other hand, $Q_{ir\text{-}pos}$ of the eight carbon materials showed a linear dependence on $2N_{H2} + N_{CO}$ (Fig. S7). Previously, such a linear correlation between $Q_{ir\text{-}pos}$ (at an upper limit potential of 1.0 V) and $2N_{H2} + N_{CO}$ was already reported by our group, without the GMS and MSC30 data [18]. It should be noted that the linear correlation between $Q_{ir\text{-}pos}$ and $2N_{H2} + N_{CO}$ (Fig. S7a) still exists even without ZTC [18]. These results suggest different mechanisms of degradation reactions at the negative and positive potential ranges. Thus, we revisited the effect of surface area. To study whether edge site or surface area produces a larger effect at the negative potential range, we focused on the two carbons in Figs. 3 and S4 as extreme models: ZTC with large surface area with a large number of edge sites, and GMS with large surface area with very few edge sites. For $Q_{ir\text{-}pos}$ (Fig. S4), the degradation-causing sites were located at the carbon edge sites. Therefore, ZTC showed large $Q_{ir\text{-}pos}$ whereas GMS showed small $Q_{ir\text{-}pos}$. On the other hand, for $Q_{ir\text{-}neg}$ (Fig. 3), both ZTC and GMS show large $Q_{ir\text{-}neg}$. Thus, it is very likely that the degradation at the negative potential range depends on the surface area rather than edge sites.

3.3. The effect of different types of carbon surface

From the above discussion, it is worth studying the relation between $Q_{ir\text{-}neg}$ and carbon surface area by nitrogen adsorption isotherm. Although the BET method is commonly used to estimate specific surface areas of carbon materials, this method has noticeable errors when applied to microporous materials in which multi-layer adsorption does not occur [36]. Alternatively, we used the pore-effect subtracting method [25] which is based on the α_s-plot, to more accurately estimate the specific surface areas (S_α). The comparison between BET surface area and S_α is shown in Table S3. Fig. 5a and b shows $Q_{ir\text{-}neg}$ of each carbon plotted against S_α in the PC-based and AN-based electrolytes. Compared to Fig. 4, better correlations were obtained, especially in 1 M Et_4NBF_4/PC.

It should be noted that S_α contains two different types of contributions: basal planes and edge sites. Since the latter has no contributions to

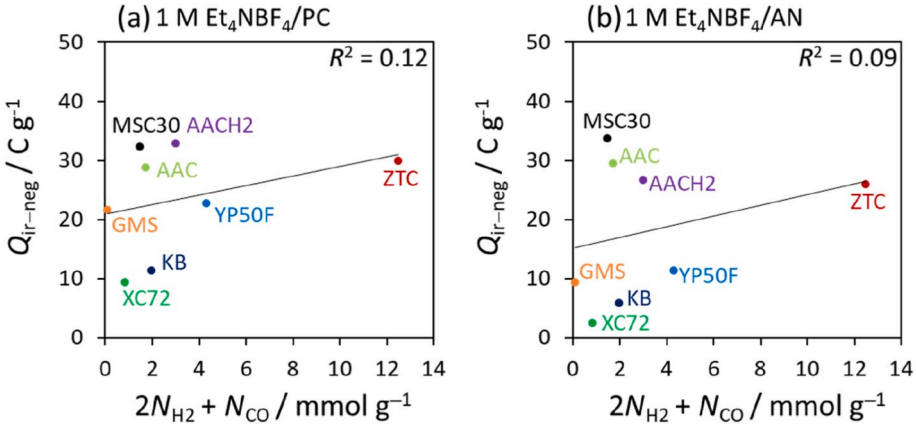

Fig. 4. The plot of $Q_{ir\text{-}neg}$ (lower limit potential of −1.5 V) against the sum of $2N_{H2}$ and N_{CO}, corresponding to the amount of edge sites terminated by H and CO-evolution groups (phenol, ether, and carbonyl group), respectively. Electrolytes are (a) 1 M Et_4NBF_4/PC and (b) 1 M Et_4NBF_4/AN.

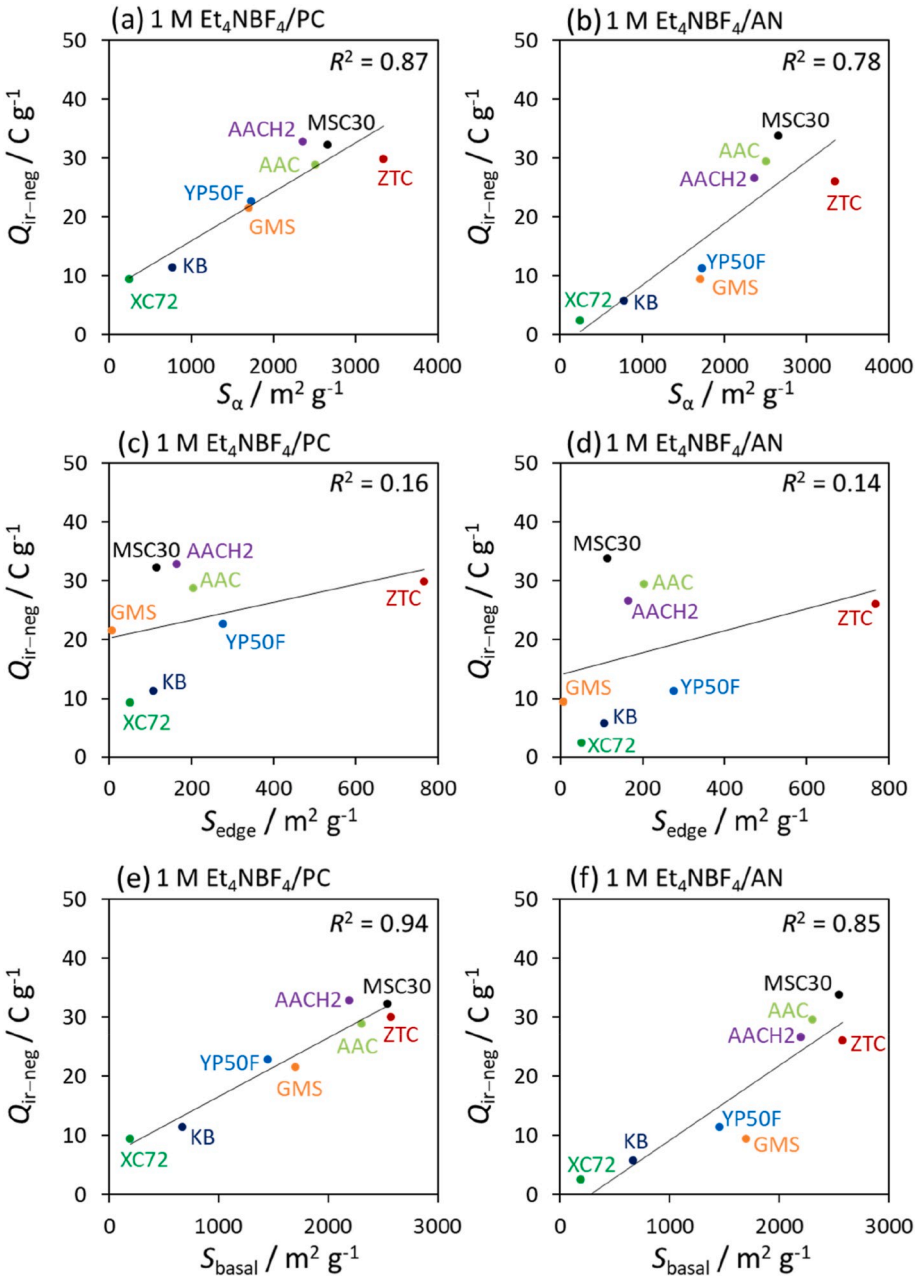

Fig. 5. The plot of $Q_{ir\text{-}neg}$ against (a,b) S_{α}, (c,d) S_{edge} and (e,f) S_{basal} in (a,c,e) 1 M Et_4NBF_4/PC and (b,d,f) 1 M Et_4NBF_4/AN.

carbon corrosion (Figs. 4a, b, S5, and S6), it is likely the basal plane may be responsible for carbon corrosion. To clarify this point, the total surface area (S_{α}) should be divided into basal-plane surface area (S_{basal}) and edge-site surface area (S_{edge}). The high-sensitive TPD up to 1800 °C enabled the quantitative determination of carbon edge sites (N_{edge} [mmol g^{-1}], shown in Table 1), and S_{edge} was calculated by assuming that the area occupied by each edge site was 0.083 nm^2 [30]. Once S_{edge} was obtained, S_{basal} can be easily calculated by subtracting S_{edge} from S_{α}. The results are shown in Table 2. Thus, $Q_{ir\text{-}neg}$ was plotted against S_{edge} (Fig. 5c and d) and S_{basal} (Fig. 5e and f). As already revealed in Figs. 4, S5, and S6, $Q_{ir\text{-}neg}$ showed no correlation with S_{edge}. On the other hand, a positive correlation was found between $Q_{ir\text{-}neg}$ and S_{basal} as shown in Fig. 5e and f. The correlation coefficients (R^2) in Fig. 5e and f ($Q_{ir\text{-}neg}$ versus S_{basal}) were better than those in Fig. 5a and b ($Q_{ir\text{-}neg}$ versus S_{α}), indicating that basal planes were responsible for the electrochemical degradation in the negative potential range.

3.4. The dependence of correlation on potential

While the above discussion was based on $Q_{ir\text{-}neg}$ at −1.5 V vs. Ag/$AgClO_4$, here we discuss how the correlation varied with the potential. The correlation coefficients (R^2) between $Q_{ir\text{-}neg}$ and different carbon surfaces (S_{α}, S_{basal} and S_{edge}) with the different lower potential limits are summarized in Fig. 6. For both electrolytes, the correlation between $Q_{ir\text{-}neg}$ and S_{α} or S_{basal} was much better than S_{edge} in the whole negative potential range. This was different from the case of positive potential range, where S_{edge} showed better correlation with $Q_{ir\text{-}pos}$ than S_{α} or S_{basal} (Fig. S8). In 1 M Et_4NBF_4/PC, the correlation between $Q_{ir\text{-}neg}$ and S_{basal} was better than that between $Q_{ir\text{-}neg}$ and S_{α}. Similar results were found in 1 M Et_4NBF_4/AN when the lower-limit potential was below −1.3 V, although the difference was small. In 1 M Et_4NBF_4/PC, R^2 for S_{basal} showed increase below −1.2 V, at which $Q_{ir\text{-}neg}$ increased (Fig. 3a). R^2 reached the maximum at −1.5 V then decreased. This decrease was mainly due to the gradual deviations of ZTC, AAC and AACH2 from the

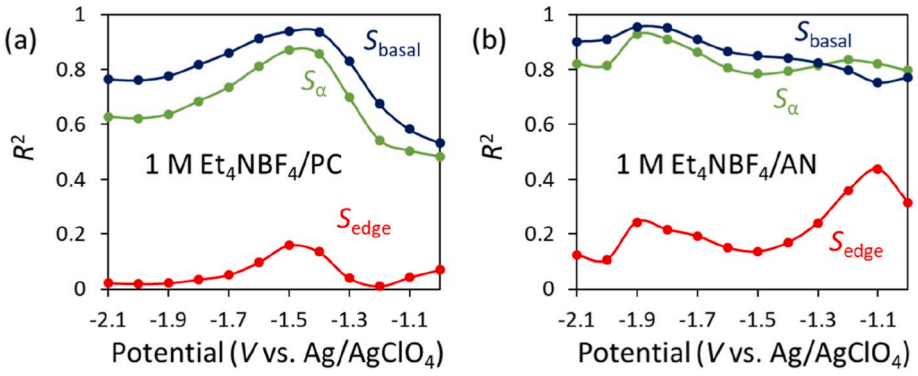

Fig. 6. Correlation coefficient (R^2) of $Q_{ir\text{-}neg}$ against carbon surfaces in different potential ranges. (a) In 1 M Et_4NBF_4/PC and (b) in 1 M Et_4NBF_4/AN.

predicted trend line. In the case of ZTC, we ascribed this phenomenon to the occurrence of pseudocapacitance. As found in Fig. S2f, only ZTC showed noticeable redox peak around −1.4 to −1 V when polarized to low potential below −1.6 V. We have previously reported a high electrochemical reactivity of ZTC at a positive potential range in the 1 M Et_4NBF_4/PC electrolyte, in which oxygen-functional groups were introduced by the oxygen contained in PC [22]. Moreover, the oxygen-doped ZTC showed a large pseudocapacitance. The highly reactive ZTC may also be electrochemically modified at the negative potential range. Because of the significant pseudocapacitance, $Q_{ir\text{-}neg}$ of ZTC deviated from the tendencies of other carbon materials especially below −1.6 V (Figs. S9a–c), making the R^2 value decreased below −1.6 V in Fig. 6a. However, the deviations of AAC and AACH2 cannot be explained from the present results and some other unknown factors may also affect the degradation process. On the other hand, the appearance of pseudocapacitance was not intense in the 1 M Et_4NBF_4/AN electrolyte (Fig. S3f), and ZTC did not deviate very much from the tendency of the $Q_{ir\text{-}neg}$–S_{basal} relation even below −1.6 V (Figs. S9d–f).

3.5. Reactant at electrolyte side

To understand the degradation mechanism, it is important to reveal not only reaction sites at carbon electrode but also the reactant in the electrolyte. In the two types of electrolytes used in this work (1 M Et_4NBF_4/PC and 1 M Et_4NBF_4/AN), the reactant is either salt (Et_4NBF_4) or solvent (PC or AN). We examined the reactivities of Et_4NBF_4, PC, and AN on YP50F by using a stable ionic liquid ($BMIMBF_4$) as a support electrolyte. Fig. 7 shows CV scans of the three components. While the CV pattern of Et_4NBF_4 was unchanged from that of the support electrolyte ($BMIMBF_4$), PC and AN showed an intense cathodic current. Thus, it was revealed that the reactant in these two electrolytes was the solvent (PC or AN) rather than the salt (Et_4NBF_4).

3.6. Computational chemistry

The experimental results indicated that carbon basal planes are more reactive than carbon edge planes at the negative potential range. To further understand the results, we investigated the electronic states and the overlapping of the molecular orbitals (MOs) for a carbon model (hexabenzocoronene) with a solvent molecule at the edge and on the basal plane of the model molecule by theoretical calculations (Fig. 8a). Acetonitrile (AN) was used as a representative of a reactant in electrolytes. As shown in Fig. 8b, the energy levels of initial HOMO state (147a) of both cases were quite similar; −6.53 eV on the basal plane and −6.52 eV at the edge site. However, there was a relatively lower lying state (159a, −3.31 eV) with an unoccupied MO delocalized over the components when AN was placed on the basal plane of the carbon model. This stabilization was not observed for the carbon model with AN at the edge (159a), and the reactant (AN) could only obtain electrons at a higher energy level (160a, −3.15 eV). This qualitatively indicated that the intermolecular electronic coupling could be stronger when AN is on the carbon basal plane, probably due to the more accessible π-electrons. Therefore the electron transfer from the negatively charged carbon model to the reactant on the basal plane ($\Delta E_{(147a-159a)} = 3.22$ eV) was more likely to occur than that at the periphery of the carbon model ($\Delta E_{(147a-160a)} = 3.37$ eV). The single-electron transfer could initiate the reductive degradation of reactants, leading to the cathodic irreversible current. Although the accurate prediction of thermodynamics and kinetics in electron transfer reactions could be achieved by the determination of the reaction coordinates that include the re-organization of solvents, the present calculations were in good agreement with the experimentally obtained results that showed the high reactivity of the

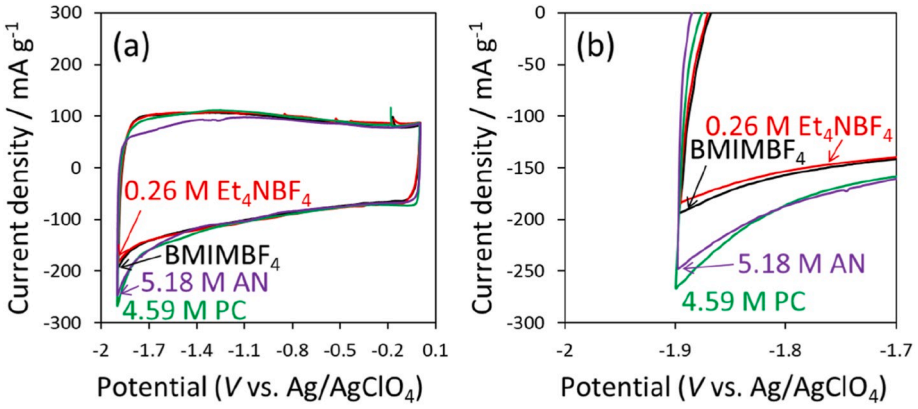

Fig. 7. (a) CV results of Et_4NBF_4, PC, and AN dissolved in a stable support electrolyte ($BMIMBF_4$). The measurement was performed by a three-electrode cell using YP50F as a working electrode at 25 °C. (b) An enlarged graph of (a) showing cathodic current around lower limit potential.

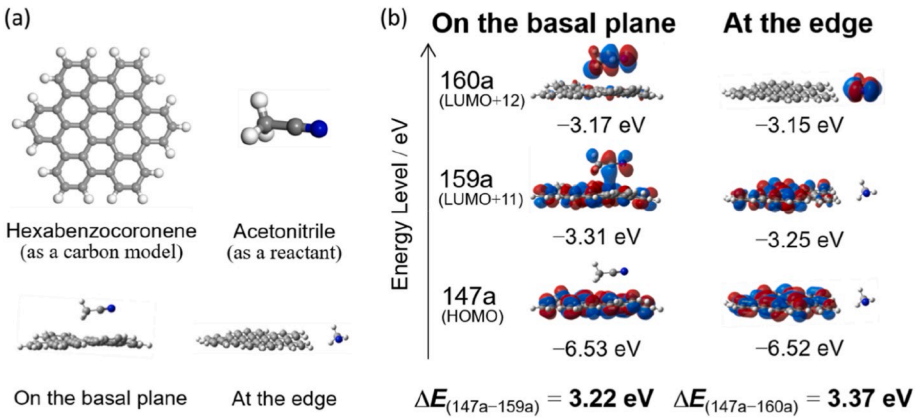

Fig. 8. (a) The structures for calculation: hexabenzocoronene as a carbon model and acetonitrile as a representative of a reactant in electrolyte. (b) Molecular orbital diagrams of a set of hexabenzocoronene (electron donor) and acetonitrile (electron acceptor) calculated at the unrestricted ωB97XD/6–311++G* level of theory. Charge: −1, Spin multiplicity: 2.

carbon basal planes compared with the edge sites.

While the experimental and theoretical investigations revealed that the initial degradation reactions were likely to occur on carbon basal planes rather than on carbon edge planes, the initial degradation reactions that this work focused on did not explore the effects on supercapacitors. We have demonstrated that there was little capacitance drop in a symmetric cell using GMS after a float test (3.5 V at 60 °C for 700 h) [8]. Although the relation between the initial degradation reactions and the life of supercapacitors remains an issue, systematic investigation on different degradation stages will provide the full understanding of a whole degradation process in future.

4. Conclusions

We investigated the degradation reactions at the negative electrode of a supercapacitor in two types of organic electrolytes (1 M Et_4NBF_4/PC or 1 M Et_4NBF_4/AN). By using eight kinds of very different carbon materials as electrode, we found that the initial degradation reactions mainly occurred at the carbon basal planes rather than the edge sites. Such tendency was also supported by theoretical calculation for a model carbon–reactant system. The results made a striking contrast to the positive potential case where carbon edge sites were responsible for the initial electrochemical degradation. This work suggests that appropriate material selection is different for positive and negative electrodes to achieve high stability of supercapacitors.

Declaration of competing interest

The authors declare that they have no known competing financial interests or personal relationships that could have appeared to influence the work reported in this paper.

CRediT authorship contribution statement

Rui Tang: Data curation, Methodology, Writing - original draft. **Masanori Yamamoto:** Formal analysis. **Keita Nomura:** Data curation. **Emilia Morallón:** Methodology. **Diego Cazorla-Amorós:** Resources, Methodology. **Hirotomo Nishihara:** Writing - review & editing, Conceptualization. **Takashi Kyotani:** Data curation, Supervision, Conceptualization.

Acknowledgements

This work was supported by JSPS KAKENHI (grant Nos. 17H01042 and 19H00913); the Dynamic Alliance for Open Innovation Bridging Human, Environment, and Materials program; and the Network Joint Research Centre for Materials and Devices. R. T. acknowledges the China Scholarship Council for the financial support. MINECO and FEDER (CTQ2015-66080-R MINECO/FEDER) are acknowledged for financial support. The computations were performed using Research Center for Computational Science, Okazaki, Japan. The authors are thankful to Dr. Tracy Chuong for her kind suggestions on English writing.

Appendix A. Supplementary data

Supplementary data to this article can be found online at https://doi.org/10.1016/j.jpowsour.2020.228042.

References

[1] B.E. Conway, Electrochemical Supercapacitors-Scientific Fundamentals and Technological Applications, Kluwer Academic, New York, 1999.
[2] D. Weingarth, A. Foelske-Schmitz, R. Kotz, J. Power Sources 225 (2013) 84–88.
[3] R. Kotz, M. Carlen, Electrochim. Acta 45 (2000) 2483–2498.
[4] P. Simon, Y. Gogotsi, Nat. Mater. 7 (2008) 845–854.
[5] P. Azaïs, L. Duclaux, P. Florian, D. Massiot, M.-A. Lillo-Rodenas, A. Linares-Solano, J.-P. Peres, C. Jehoulet, F. Béguin, J. Power Sources 171 (2007) 1046–1053.
[6] M. Hahn, A. Würsig, R. Gallay, P. Novák, R. Kötz, Electrochem. Commun. 7 (2005) 925–930.
[7] R. Kötz, M. Hahn, R. Gallay, J. Power Sources 154 (2006) 550–555.
[8] K. Nomura, H. Nishihara, N. Kobayashi, T. Asada, T. Kyotani, Energy Environ. Sci. 12 (2019) 1542–1549.
[9] D. Weingarth, H. Noh, A. Foelske-Schmitz, A. Wokaun, R. Kötz, Electrochim. Acta 103 (2013) 119–124.
[10] M.A. Sakka, H. Gualous, J.V. Mierlo, H. Culcu, J. Power Sources 194 (2009) 581–587.
[11] A. Izadi-Najafabadi, S. Yasuda, K. Kobashi, T. Yamada, D.N. Futaba, H. Hatori, M. Yumura, S. Iijima, K. Hata, Adv. Mater. 22 (2010) E235–E241.
[12] A. Yoshida, I. Tanahashi, A. Nishino, Carbon 28 (1990) 611–615.
[13] C.H. Yang, Q.D. Nguyen, T.H. Chen, A.S. Helal, J. Li, J.K. Chang, ACS Sustain. Chem. Eng. 6 (2018) 1208–1214.
[14] S. Ishimoto, Y. Asakawa, M. Shinya, K. Naoi, J. Electrochem. Soc. 156 (2009) A563–A571.
[15] M. Hahn, R. Kötz, R. Gallay, A. Siggel. Electrochim. Acta 52 (2006) 1709–1712.
[16] D. Cazorla-Amorós, D. Lozano-Castelló, E. Morallón, M.J. Bleda-Martínez, A. Linares-Solano, S. Shiraishi, Carbon 48 (2010) 1451–1456.
[17] M. Zhu, C.J. Weber, Y. Yang, M. Konuma, U. Starke, K. Kern, A.M. Bittner, Carbon 46 (2008) 1829–1840.
[18] R. Tang, K. Taguchi, H. Nishihara, T. Ishii, E. Morallón, D. Cazorla-Amorós, T. Asada, N. Kobayashi, Y. Muramatsu, T. Kyotani, J. Mater. Chem. A 7 (2019) 7480–7488.
[19] J. Li, Z. Xu, Z.A. Zhang, RSC Adv. 8 (2018) 32188–32192.
[20] K. Xu, M.S. Ding, T.R. Jow, Electrochim. Acta 46 (2001) 1823–1827.
[21] P.W. Ruch, D. Cericola, A. Foelske, R. Kötz, A. Wokaun, Electrochim. Acta 55 (2010) 2352–2357.
[22] K. Nueangnoraj, H. Nishihara, T. Ishii, N. Yamamoto, H. Itoi, R. Berenguer, R. Ruiz-Rosas, D. Cazorla-Amorós, E. Morallón, M. Ito, T. Kyotani, Energy Storage Mater 1 (2015) 35–41.
[23] H. Nishihara, T. Simura, S. Kobayashi, K. Nomura, R. Berenguer, M. Ito, M. Uchimura, H. Iden, K. Arihara, A. Ohma, Y. Hayasaka, T. Kyotani, Adv. Funct. Mater. 26 (2016) 6418–6427.
[24] R.D. Heidenre, W.M. Hess, L.L. Ban, J. Appl. Crystallogr. 1 (1968) 1–19.

[25] K. Kaneko, C. Ishii, M. Ruike, H. Kuwabara, Carbon 30 (1992) 1075–1088.
[26] K. Matsuoka, Y. Yamagishi, T. Yamazaki, N. Setoyama, A. Tomita, T. Kyotani, Carbon 43 (2005) 876–879.
[27] T. Ishii, S. Kashihara, Y. Hoshikawa, J. Ozaki, N. Kannari, K. Takai, T. Enoki, T. Kyotani, Carbon 80 (2014) 135–145.
[28] L.R. Radovic, B. Bockrath, J. Am. Chem. Soc. 127 (2005) 5917–5927.
[29] T. Enoki, K. Takai, Solid State Commun. 149 (2009) 1144–1150.
[30] N.R. Laine, F.J. Vastola, P.L. Walker, J. Phys. Chem. 67 (1963) 2030–2034.
[31] K. Xu, S.P. Ding, T.R. Jow, J. Electrochem. Soc. 146 (1999) 4172–4178.
[32] M.J. Frisch, et al., Gaussian 09 Revision B.01, Gaussian Inc., Wallingford, CT, 2010.
[33] A.D. Becke, J. Chem. Phys. 107 (1997) 8554–8560.
[34] J.D. Chai, M. Head-Gordon, Phys. Chem. Chem. Phys. 10 (2008) 6615–6620.
[35] A. Klamt, G. Schuurmann, J. Chem. Soc., Perkin Trans. 2 (1993) 799–805.
[36] K. Kaneko, C. Ishii, Colloids Surf 67 (1992) 203–212.
[37] D. Lozano-Castello, M.A. Lillo-Rodenas, D. Cazorla-Amoros, A. Linares-Solano, Carbon 39 (2001) 741–749.